



**HAL**  
open science

# Cation-deficient Ca-doping lanthanum tungstate $\text{Ca}_{2.06}\text{La}_{2.61}\text{O}_{12}$ : structure and transport property study

Qiong Ye, Maud Barré, Karim Adil, A Rousseau, Emmanuelle Suard, F  
Goutenoire

► **To cite this version:**

Qiong Ye, Maud Barré, Karim Adil, A Rousseau, Emmanuelle Suard, et al.. Cation-deficient Ca-doping lanthanum tungstate  $\text{Ca}_{2.06}\text{La}_{2.61}\text{O}_{12}$ : structure and transport property study. Journal of Solid State Chemistry, 2022, 313, pp.123310. 10.1016/j.jssc.2022.123310 . hal-03691614

**HAL Id: hal-03691614**

**<https://hal.science/hal-03691614>**

Submitted on 9 Jun 2022

**HAL** is a multi-disciplinary open access archive for the deposit and dissemination of scientific research documents, whether they are published or not. The documents may come from teaching and research institutions in France or abroad, or from public or private research centers.

L'archive ouverte pluridisciplinaire **HAL**, est destinée au dépôt et à la diffusion de documents scientifiques de niveau recherche, publiés ou non, émanant des établissements d'enseignement et de recherche français ou étrangers, des laboratoires publics ou privés.

# Cation-deficient Ca-doping lanthanum tungstate $\text{Ca}_{2.06}\text{La}_{2.61}\square_{0.33}\text{W}_2\text{O}_{12}$ : structure and transport property study

Q. Ye<sup>a</sup>, M. Barré<sup>a</sup>, K. Adil<sup>a</sup>, A. Rousseau<sup>a</sup>, E. Suard<sup>b</sup> and F. Goutenoire<sup>a</sup>

<sup>a</sup> IMMM (Institut des Molécules et Matériaux du Mans), UMR-CNRS 6283, Le Mans Université, 72085 Le Mans Cedex 9, France.

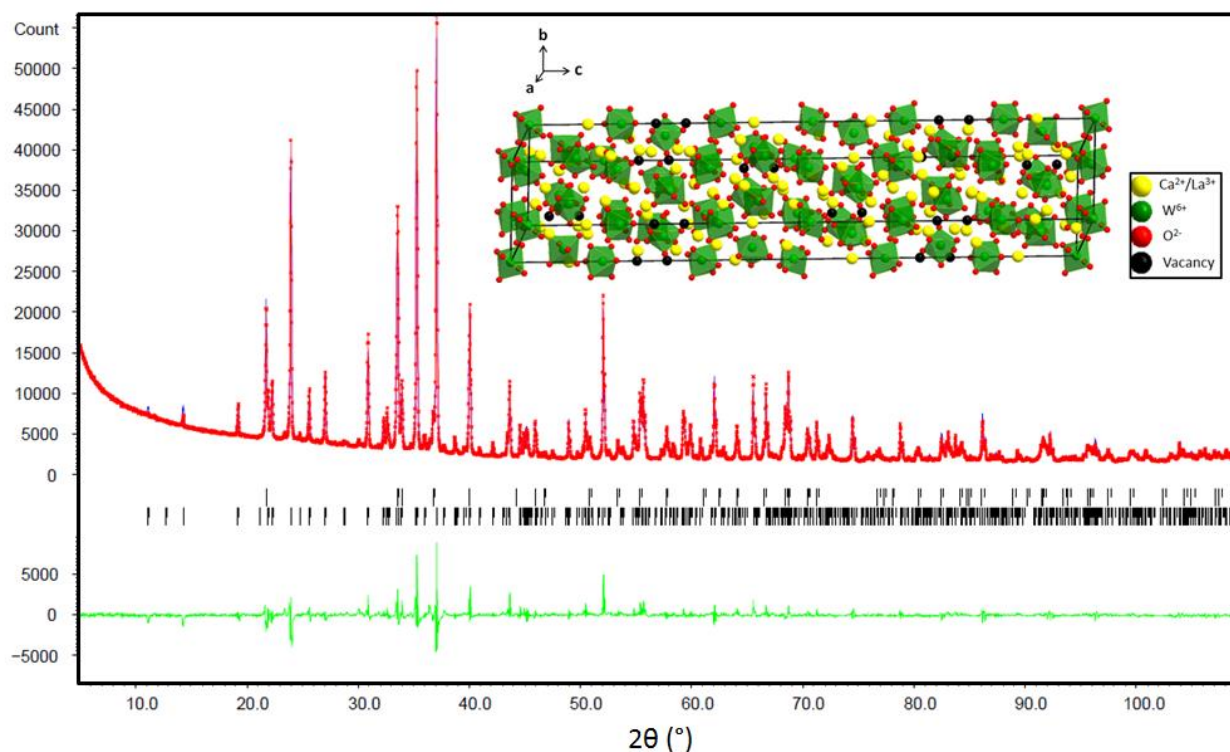
<sup>b</sup> ILL (Institut Laue Langevin), Avenue des Martyrs, B. P. 156, 38042 Grenoble Cedex, France.

## Abstract

A new cation-deficient Ca-doping lanthanum tungstate compound with the exact formula  $\text{Ca}_{2.06}\text{La}_{2.61}\square_{0.33}\text{W}_2\text{O}_{12}$  ( $\square$  indicating a vacancy) is presented in this work. It crystallizes in the space group  $R\bar{3}C$  (No.167),  $Z = 18$  with the hexagonal parameters  $a = 9.7747(1) \text{ \AA}$  and  $c = 55.7833(4) \text{ \AA}$ , similar to  $\text{Ca}_5\text{Re}_2\text{O}_{12}$ . This compound belongs to a rare small crystallographic family  $A_5B_2X_{12}$  having large cells. The thermodynamic and kinetic processes of synthesizing this white powder compound are very slow. Its structure is analyzed by X-ray, neutron powder and electron diffraction. The conduction properties are investigated with complex impedance spectroscopy.

## Graphical abstract

A new cation-deficient Ca-doping lanthanum tungstate was discovered with the exact formula  $\text{Ca}_{2.06}\text{La}_{2.61}\square_{0.33}\text{W}_2\text{O}_{12}$ . The crystallographic structure was solved. This compound belongs to a rare small crystallographic family  $A_5B_2X_{12}$  having large cells, and presents a weak ionic conductivity in both dry and humid air atmosphere.



## Keywords

X-ray and neutron powder diffraction; Electron diffraction; Ion doping; Cation deficiency; Ionic conduction.

## 1. Introduction

In the current ecological and economic context, Fuel Cells (FCs) represent a promising technology as a clean, efficient and renewable energy source which is a potential alternative to fossil fuels. Electrolyte being one of the core elements of FCs, finding new materials with higher performance, higher reliability and lower cost is the key to improve these devices. A proposed line of research is the development of new solid electrolytes which have many advantages compared with liquid electrolytes: excellent mechanical resistance, easy to mould, higher reliability and security as well as higher energy density, and so on.

In recent years, a family of compounds called LAMOX, derived from  $\text{La}_2\text{Mo}_2\text{O}_9$  which is a potential solid electrolyte material applicable to Solid Oxide Fuel Cells (SOFCs), has attracted much attention.  $\text{La}_2\text{Mo}_2\text{O}_9$  possesses high oxide ion conductivity at high temperature <sup>[1][2][3]</sup> similar to the state-of-the-art solid electrolyte for SOFCs: Yttria-stabilized Zirconia (YSZ) <sup>[4][5][6]</sup>. However, the conductivity of these high-quality electrolyte materials sharply decreases with decreasing temperature. So SOFCs can only operate at high temperatures. Such conditions are inevitably associated with many drawbacks limiting SOFCs commercialization, such as restriction of the compatible cell materials, unacceptable performance and electrode degradation rates, requirement of large input energy to heat the cell stacks, long start-up and shut-down cycles and so on <sup>[7][8][9][10]</sup>. In order to increase SOFCs competitiveness, it is necessary to lower the operating temperature down to the intermediate temperature (IT) range (600°C-800°C) or even to the low temperature (LT) range (400°C-600°C). Consequently, there is an urgent need to develop electrolytes able to maintain sufficiently high electrochemical activity in the targeted range of temperature between 400°C and 600°C. In addition,  $\text{La}_2\text{Mo}_2\text{O}_9$  exhibits a reversible phase transition between the low temperature  $\alpha$ -polymorph (monoclinic) and the high temperature  $\beta$ -polymorph (cubic) at 560°C <sup>[2][3][11]</sup>, leading to further conductivity decrease at low temperatures. Hence, stabilizing the high temperature crystal structure is also an important research topic <sup>[12][13][14][15]</sup>. As we know, an excellent electrolyte material must meet the following conditions: large number of mobile species and vacancies, 3D conductive network, low barrier between the occupied sites and the empty sites, and strongly polarizable ions. It is clear that creating enough vacancies within the crystal structure to form 3D pathways facilitating the transport of the mobile species is a good approach to improve ionic conductivity. Substitution is a widely used method in the field of crystallography for creating vacancies within the crystal structure while stabilizing the structure.

In the last two decades, the complete and partial substitutions of  $\text{La}^{3+}$  and/or  $\text{Mo}^{6+}$  with the same and/or lower valence ions such as  $\text{W}^{6+}$ ,  $\text{Nb}^{5+}$ ,  $\text{Bi}^{3+}$ ,  $\text{Sr}^{2+}$ ,  $\text{Ba}^{2+}$ ,  $\text{K}^+$  and so on, have been widely studied <sup>[13][15][16][17]</sup>. In view of the similar ionic radius of  $\text{Mo}^{6+}$  and  $\text{W}^{6+}$ , equal to 0.59 and 0.60 Å, respectively,  $\text{La}_2\text{W}_2\text{O}_9$  can be considered as a compound in which  $\text{Mo}^{6+}$  is completely substituted by  $\text{W}^{6+}$ .  $\text{La}_2\text{W}_2\text{O}_9$  also exhibits two different crystallographic polymorphs:  $\alpha$ -triclinic at low temperature and  $\beta$ -cubic at high temperature, the reversible phase transition occurring at about 1070°C <sup>[18][19]</sup>. Similarly,  $\beta$ - $\text{La}_2\text{W}_2\text{O}_9$  presents an ionic conductivity of the same order of magnitude as  $\beta$ - $\text{La}_2\text{Mo}_2\text{O}_9$  in the high temperature range ( $T > 1080^\circ\text{C}$ ) <sup>[12]</sup>. The binary system  $\text{La}_2\text{O}_3 - \text{WO}_3$  also presents other conductive compounds. Examples include  $\text{La}_6\text{WO}_{12}$  in the work of Haugsrud and Kjolseth which presents a protonic conduction ( $\sigma = 3 \times 10^{-3} \text{ S cm}^{-1}$  at approximately 800°C in wet  $\text{H}_2$ ) <sup>[20]</sup> with a face centred cubic structure <sup>[21]</sup>, and  $\text{La}_{10}\text{W}_2\text{O}_{21}$  in the work of M. H. Chambrier *et al.* which presents an oxide ionic conduction ( $10^{-4} - 10^{-3} \text{ S cm}^{-1}$  at 800°C – 1000°C in dry air atmosphere) with the anion-deficient fluorite related superstructure <sup>[22]</sup>. On the other hand, the partial substitution of  $\text{Mo}^{6+}$  with  $\text{W}^{6+}$  has also been studied in the work of D. Marrero-Lopez *et al.* on the conduction of  $\text{La}_2\text{Mo}_{2-x}\text{W}_x\text{O}_9$  materials <sup>[14]</sup>. The introduction of third ion has been also studied,

an example is the substitution of  $\text{La}^{3+}$ ,  $\text{Mo}^{6+}$  and/or  $\text{W}^{6+}$  with  $\text{Nb}^{5+}$  carried out by T.D. Vu *et al.* [17][23]. But none of the new materials they found exhibited satisfactory ionic conductivity.

As is well known, the greater the valence difference between doping ions and substituted ions, the more vacancies can be created to maintain the charge neutrality of the compound when doping occurs. Considering the low valence of calcium ion (+2) and its valence differences of 1 and 4 with  $\text{La}^{3+}$  and  $\text{W}^{6+}$ , respectively, we focus on the synthesis of lanthanum tungstate doped with  $\text{Ca}^{2+}$  in this work with the aim of finding new compounds having larger stability and conductivity.

## 2. Experimental section

The compound was synthesized with three starting oxides  $\text{La}_2\text{O}_3$ ,  $\text{WO}_3$  and  $\text{CaCO}_3$  by conventional solid state ceramic route. Prior to use,  $\text{La}_2\text{O}_3$  was dried and decarbonated at  $1000^\circ\text{C}$  overnight. The different oxides were weighted in the stoichiometric proportions: 43%  $\text{CaCO}_3$  - 23%  $\text{La}_2\text{O}_3$  - 34%  $\text{WO}_3$ , and ground together with ethanol as dispersant in an agate mortar. The dry mixed powder was heated at  $1400^\circ\text{C}$  for several days in an alumina crucible with many intermediate grindings.

The room temperature X-ray powder diffraction data was collected on a Bragg-Brentano geometry diffractometer (MPD-PRO Panalytical) from  $5^\circ$  to  $110^\circ$  ( $2\theta$ ) with a step of  $0.017^\circ$  for about 2 hours with a cobalt radiation ( $\lambda = 1.7903 \text{ \AA}$ ).

Neutron diffraction data was collected on the powder diffractometer D2B instrument at ILL in Grenoble, France, at constant wavelength  $\lambda \approx 1.5941 \text{ \AA}$  and room temperature on about 15g of compressed powder. For the pattern, the increment step is  $0.05^\circ$  ( $2\theta$ ) in the range of  $5^\circ - 160^\circ$ ; the total counting time is about 2 hours.

The electron diffraction study was performed on a 200 kV side entry JEOL2100 transmission electron microscope with a double-tilt specimen holder operating at room temperature.

For electrical measurements, the pellets of 8 millimeters in diameter and around 2 millimeters thickness were recompressed with iso-static pressure of 5000 bars. For determining the optimal sintering temperature, dilatometry analysis was performed on Setsys Evolution 1750 (TMA Alumina) in the temperature range  $20^\circ\text{C} - 1450^\circ\text{C}$  in the air atmosphere. The morphology of sintered pellet was studied on a 20 kV JEOL (JSM 6510 LV) scanning electron microscope (SEM). The pellet used to measure the conductivity was sintered first and then a thin platinum layer as electrode was deposited on both faces by plasma spraying. The ionic conductivity was measured by complex impedance spectroscopy in the 10 MHz to 1 Hz frequency range with alternative voltage of 500 mV amplitude, by using a Schlumberger Solartron SI 1260 frequency response analyzer connected to a solartron 1296 dielectric interface with Smart [24] impedance software for data collection in dry air and humid air atmosphere.

## 3. Results and discussion

### 3.1 Thermal treatment

In order to obtain about 20g of pure compound from the stoichiometric proportions of  $\text{Ca}_{2.06}\text{La}_{2.61}\text{W}_2\text{O}_{12}$ : 38.5%  $\text{CaCO}_3$  - 24.3%  $\text{La}_2\text{O}_3$  - 37.2%  $\text{WO}_3$ , a very long thermal treatment is necessary. The three steps of thermal treatment, the corresponding conditions, the Rietveld refinement diffraction pattern from X-ray data and the figures of merit of refinements are shown in the **Table 1**.

Steps and conditions	Figures of merit of refinement	Rietveld refinement diffraction patterns from X-ray data
The first step:  1300°C for 50 hours is followed by 1400°C for 40 hours.	$R_{\text{Bragg}}(\text{Ca}_2\text{La}_3\text{W}_2\text{O}_{12}) = 5.89\%$ $R_{\text{Bragg}}(\text{CaWO}_4) = 3.69\%$	
	$R_p = 6.64\%$ $R_{\text{wp}} = 9.21\%$	
The second step:  1400°C for 300 hours.	$R_{\text{Bragg}}(\text{Ca}_2\text{La}_3\text{W}_2\text{O}_{12}) = 2.52\%$ $R_{\text{Bragg}}(\text{CaWO}_4) = 2.92\%$	
	$R_p = 5.93\%$ $R_{\text{wp}} = 8.31\%$	
The third step:  1400°C for 130 hours.	$R_{\text{Bragg}}(\text{Ca}_2\text{La}_3\text{W}_2\text{O}_{12}) = 3.72\%$	
	$R_p = 6.63\%$ $R_{\text{wp}} = 9.77\%$	

**Table 1:** Description of the three steps of thermal treatment, the Rietveld refinement diffraction pattern from X-ray data and the figures of merit of refinements.  $\text{Ca}_2\text{La}_3\text{W}_2\text{O}_{12}$  in the legend of the figures is a simplified formula of  $\text{Ca}_{2.06}\text{La}_{2.61}\text{W}_{2.03}\text{O}_{12}$ .  $R_{\text{Bragg}}$ : Bragg residual;  $R_p$ : profile residual (reliability);  $R_{\text{wp}}$ : weighted profile residual.

This long and slow thermal treatment is associated with important thermodynamic and kinetic processes for getting a pure form of the title compound. It is to note the white color of the final powder.

### 3.2 Electron diffraction

The first crystallographic analysis was carried out via a combination of the electron and laboratory X-ray diffraction data. By using the auto-indexation program DICVOL04<sup>[25]</sup> implemented in the software HighScorePlus<sup>[26]</sup>, the following hexagonal cell parameters was extracted from X-ray diffraction data:  $a = 9.760 \text{ \AA}$ ,  $c = 55.739 \text{ \AA}$  and  $V = 4597.60 \text{ \AA}^3$ , with  $F_{30} = 17$ <sup>[27]</sup>. The general formulation of the new compound was extrapolated by the nominal composition: 36% CaO – 27%  $\text{La}_2\text{O}_3$  – 36%  $\text{WO}_3$ :  $(36x\text{CaO}) (27x\text{La}_2\text{O}_3) (36x\text{WO}_3) = \text{Ca}_{36}\text{La}_{54}\text{W}_{36}\text{O}_{225}$ . The number of chemical units per unit cell  $Z = 18$  is easily deduced because  $\text{Ca}_{36}\text{La}_{54}\text{W}_{36}\text{O}_{225} / 18 \approx \text{Ca}_2\text{La}_3\text{W}_2\text{O}_{12}$ . This result is confirmed by the calculation of the volume of unit oxygen atom of the compound:  $4597.5970 / (12 \times 18) \approx 21 \text{ \AA}^3$ , which is perfectly in accordance with the average volume of oxygen atom in oxides:  $18 - 22 \text{ \AA}^3$ .

The electron diffraction patterns (TEM) revealed a hexagonal cell with the parameters  $a \approx 9.8 \text{ \AA}$  and  $c \approx 55.8 \text{ \AA}$ , which are quite close to the values given by the auto-indexation from X-ray diffraction data. The reconstruction of reciprocal

lattice was interpreted on the plan  $(\bar{1}00)^*$  containing  $\vec{b}^*$  and  $\vec{c}^*$  (Figure 1). The calculated electron diffraction pattern was performed with CrysTBox [28].

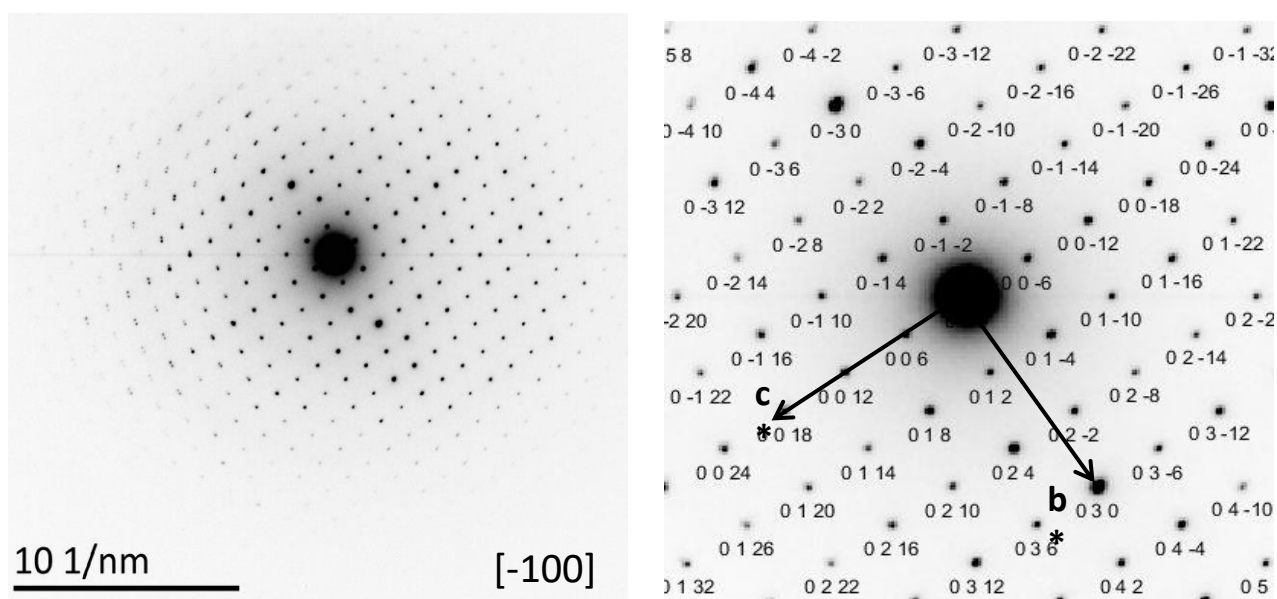


Figure 1: Electron diffraction pattern of  $[-100]$  plan of the hexagonal cell.

To determine the space group of this compound, Le Bail refinement procedure [29] was applied with the space group  $R\bar{3}m$  (No.160) using the Fullprof program [30]. Clearly, careful examination of the extracted reflection list revealed the presence of the following condition  $00l: l = 6n$ , which implies that the space group can be either  $R\bar{3}C$  (No.161) or  $R\bar{3}C$  (No.167).

Starting from both unit cell parameters and deduced space groups, we looked-for plausible isotypes within the Inorganic Crystal Structure Database (ICSD) having the general formula  $A_2B_5X_{12}$ . Four isotypes of the new compound which crystallize in the space group  $R\bar{3}C$  (No.167) were found and are listed in the table hereafter (Table 2).

Compound	a (Å)	c (Å)	V (Å <sup>3</sup> )	Ref.
Ca <sub>5</sub> Re <sub>2</sub> O <sub>12</sub>	9.5536(8)	54.586(4)	4314.65	[31]
Sr <sub>5</sub> Re <sub>2</sub> O <sub>12</sub>	9.9530(7)	56.707(3)	4864.92	[31]
Ca <sub>5</sub> (IO <sub>6</sub> ) <sub>2</sub>	9.6257(2)	54.6451(14)	4384.77	[32]
Sr <sub>5</sub> (IO <sub>6</sub> ) <sub>2</sub>	10.0164(3)	56.884(3)	4942.47	[32]
Ca <sub>2</sub> La <sub>3</sub> W <sub>2</sub> O <sub>12</sub>	9.7797(1)	55.8229(8)	4623.70	present work

Table 2: List of the isotypic compounds  $A_2B_5X_{12}$ .

### 3.3 Rietveld refinement and structure analysis

The combined Rietveld refinements were carried out from X-ray and neutron powder diffractions of the sample (43% CaCO<sub>3</sub> - 23% La<sub>2</sub>O<sub>3</sub> - 34% WO<sub>3</sub>) by using JANA program [33]. The initial structural model used for our new compound was the isotype Ca<sub>5</sub>Re<sub>2</sub>O<sub>12</sub> reported by H. A. Mons *et al.* [31]. The refinement of the structure was performed with mixed sites (Ca/La). The mixed X-ray and neutron Rietveld refinements of the appropriate atomic coordinates, temperature factors, cell parameters, specimen displacement, peak shape and background parameters lead to the global parameters in Table 3 and the atomic parameters in Table 4. Correction of roughness for the Bragg-Brentano geometry [34] was performed for the X-

ray data in order to limit the negative temperature factor of the heavy atoms W and La, which is the consequence of their large linear absorption coefficient:  $\mu_{\text{Co}} = 2044.41 \text{ cm}^{-1}$ . Thirty-seven parameters were refined. From the final result of the structural refinement we can deduce the global formula  $\text{Ca}_{2.06}\text{La}_{2.61}\square_{0.33}\text{W}_2\text{O}_{12}$ , with the oxidation state of calcium  $\text{Ca}^{2+}$ , lanthanum  $\text{La}^{3+}$  and tungsten  $\text{W}^{6+}$ . The occupation rate of cation vacancy is  $0.33 / (2.06+2.61+0.33+2) \approx 4.72\%$ . A large proportion of impurity  $\text{CaWO}_4$  (Scheelite) with the mass ratio 0.163(5) and 0.1875(15) for neutron and XRD data refinement, respectively. The refined Rietveld plots are shown in **Figure 2** and **Figure 3**.

Diffractionmeter	MPD-PRO	D2B(ILL)
Radiation (Å)	Co-K $\alpha$	1.59406(4)
2 $\theta$ range (°)	5-110	5-160
Step (°)	0.017	0.05
Total measurement time	~ 2h	~ 2h
GOF	3.84	3.26
R <sub>p</sub> (%)	4.05	4.45
R <sub>wp</sub> (%)	6.05	6.16
R <sub>Bragg</sub> (%)	8.52	5.01
R <sub>exp</sub> (%)	1.58	1.89
hkl number	416	1026

**Table 3:** Global result of the Rietveld refinement of X-ray data and neutron data.

$\text{Ca}_{2.06}\text{La}_{2.61}\square_{0.33}\text{W}_2\text{O}_{12}$ ,  $R\bar{3}C$  (No.167),  $Z = 18$ ,  $a = 9.7747(1)$  (Å),  $c = 55.7833(4)$  (Å)

Atom	site	x	y	z	B-mixed (Å <sup>2</sup> )	Occ.
Ca1/La1	36f	0.0141(4)	0.3740(3)	0.1880(1)	0.43(6)	0.76(1)/0.24(1)
Ca2/La2	36f	0.3824(2)	0.0534(2)	0.0494(1)	0.69(4)	0.22(1)/0.78(1)
Ca3/La3	12c	0.0000	0.0000	0.1033(1)	0.31(7)	0.15(1)/0.85(1)
W1	18e	0.3302(2)	0.0000	0.2500	0.51(4)	1.00
W2	12c	0.0000	0.0000	0.1626(1)	0.60(6)	1.00
W3	6b	0.0000	0.0000	0.0000	0.69(9)	1.00
O1	36f	0.0005(5)	0.2025(4)	0.2228(1)	0.41(6)	1.00
O2	36f	0.0010(5)	0.1642(5)	0.0195(1)	0.44(5)	1.00
O3	36f	0.1224(5)	0.1900(5)	0.1784(1)	0.62(6)	1.00
O4	36f	0.1817(4)	0.0661(4)	0.1397(1)	0.28(6)	1.00
O5	36f	0.1857(4)	0.3113(4)	0.1067(1)	0.45(6)	1.00
O6	36f	0.2536(4)	0.1095(4)	0.0827(1)	0.27(6)	1.00

**Table 4:** Atomic parameter results of the combined Rietveld refinement of X-ray data and neutron data.

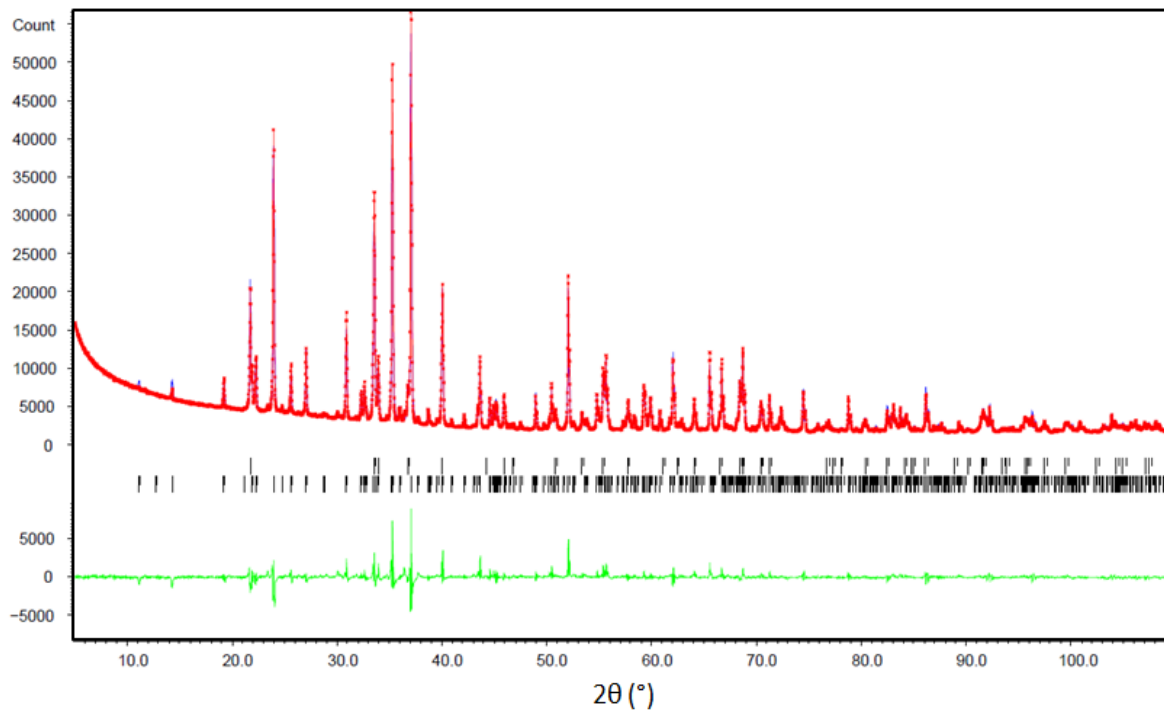


**Figure 2:** Combined Rietveld refinement diffraction pattern from X-ray data. The red crosses represent the observed data; the blue line represents the calculated ones; the black sticks are the peaks position (lower: Ca<sub>2.06</sub>La<sub>2.61</sub>□<sub>0.33</sub>W<sub>2</sub>O<sub>12</sub>, and upper: CaWO<sub>4</sub>); and the green curve shows the difference between the observed and calculated patterns.

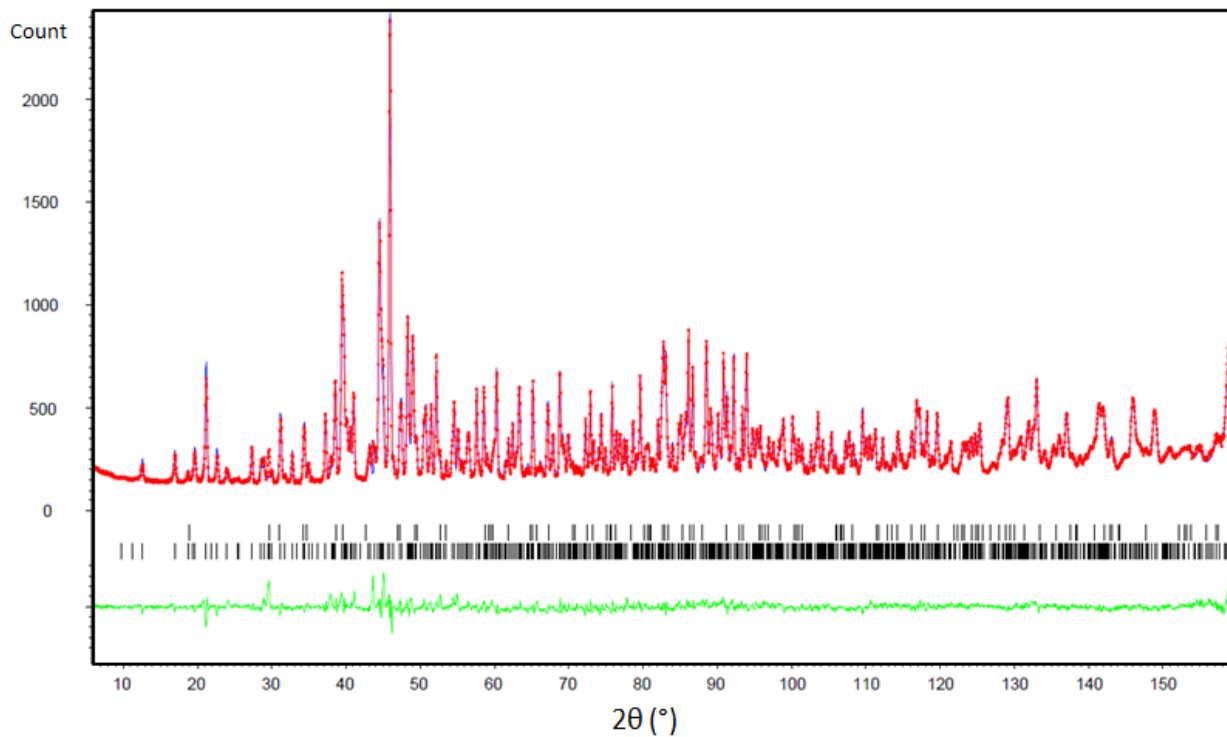


**Figure 3:** Combined Rietveld refinement diffraction pattern from neutron data. The red crosses represent the observed data; the blue line represents the calculated ones; the black sticks are the peaks position (lower: Ca<sub>2.06</sub>La<sub>2.61</sub>□<sub>0.33</sub>W<sub>2</sub>O<sub>12</sub>, and upper: CaWO<sub>4</sub>); and the green curve shows the difference between the observed and calculated patterns.

The bond valence sum calculations (BVC) were made manually with the atomic positions and occupancies determined from the combined Rietveld refinement, by using the Brown-Altarmatt empirical expression<sup>[35]</sup>:  $\text{Valence} = \sum \exp[(Ro - d)/B]$  with  $B = 0.37 \text{ \AA}$ , the values of  $Ro$  are  $2.172 \text{ \AA}$  for  $\text{La}^{3+} - \text{O}^{2-}$ ,  $1.917 \text{ \AA}$  for  $\text{W}^{6+} - \text{O}^{2-}$  and  $1.967 \text{ \AA}$  for  $\text{Ca}^{2+} - \text{O}^{2-}$ . The calculated values show a good agreement with the expected values (see **Table 5**). The interatomic distances in the structure obtained from the mixed Rietveld refinement are listed in **Table 6**.

Atom	expected valence	Calculated valence	Atom	expected valence	Calculated valence
Ca1/La1	2.32*	2.11	O1	2	1.91
Ca2/La2	2.78*	2.98	O2	2	1.88
Ca3/La3	2.85*	2.66	O3	2	2.12
W1	6	5.97	O4	2	1.95
W2	6	6.10	O5	2	2.05
W3	6	5.86	O6	2	2.20

**Table 5:** Values of the calculated and expected bond valences for the atoms.  
\* indicates the expected valence corresponding to the average valence for the mixed sites.

Atom	$D_{\text{bond}} (\text{\AA})$	Atom	$D_{\text{bond}} (\text{\AA})$	Atom	$D_{\text{bond}} (\text{\AA})$	Atom	$D_{\text{bond}} (\text{\AA})$				
Ca1/La1	O1	2.521(5)	Ca2/La2	O1	2.466(5)	Ca3/La3	O4 (X3)	2.549(5)	W1	O1 (X2)	1.970(3)
	O2	2.672(5)		O1	2.514(5)		O5 (X3)	2.655(3)	W1	O5 (X2)	1.887(5)
	O2	2.500(4)		O2	2.573(5)		O6 (X3)	2.450(4)	W1	O6 (X2)	1.916(3)
	O2	2.755(5)		O3	2.520(4)				W2	O3 (x3)	1.844(5)
	O3	2.555(6)		O4	2.440(5)				W2	O4 (X3)	2.003(5)
	O3	2.478(6)		O5	2.513(4)				W3	O2 (X6)	1.930(4)
	O4	2.390(4)		O6	2.454(5)						
	O5	2.419(5)		O6	2.548(5)						

**Table 6:** Interatomic distances ( $\text{\AA}$ )

The coordination environment of the different cations presents the following features: the calcium and lanthanum ions are distributed in a mixed form, the Ca1/La1 and Ca2/La2 situated on the 36f-sites have eight oxygen neighbors with irregular arrangements, and Ca3/La3 are located on the 12c-sites sharing nine oxygen neighbors. The three W sites 18e, 12c and 6b are all octahedrally coordinated to six oxygen atoms in the form of  $[\text{WO}_6]$ , the octahedral are mutually independent. The 6a-site is vacant. The structure is illustrated in **Figure 4**.

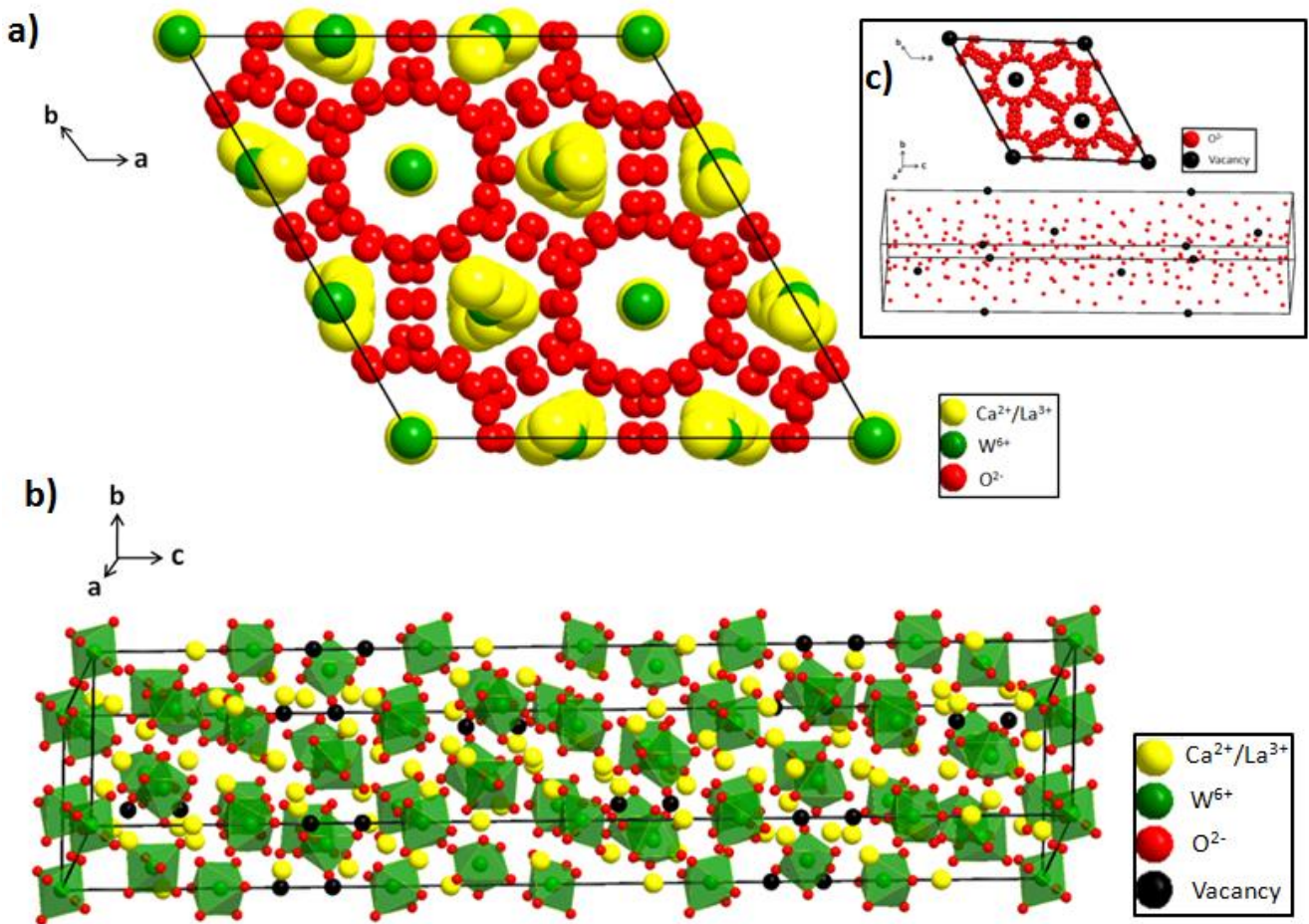


**Figure 4:** Projection of the hexagonal structure along [001] (a) and [-100] (b); (c) corresponds to the distributions of the oxygen atoms and the vacancies. Legend: yellow spheres - mixed sites of Ca/La; green sphere-W; green octahedral-[WO<sub>6</sub>]; red sphere-O; black sphere-vacancy of cation.

The result of the combined Rietveld refinement of  $\text{Ca}_{2.06}\text{La}_{2.61}\square_{0.33}\text{W}_2\text{O}_{12}$  shows the occupancy of the 6a-site is close to zero while this site is fully occupied by Ca4 for  $\text{Ca}_5\text{Re}_2\text{O}_{12}$ . This signifies that the 6a-site is probably a cationic vacancy for  $\text{Ca}_{2.06}\text{La}_{2.61}\square_{0.33}\text{W}_2\text{O}_{12}$ . The previous study shows that the distance of Ca4 — O (2.305 Å) is the shortest among all the Ca — O distances in the structure of  $\text{Ca}_5\text{Re}_2\text{O}_{12}$ <sup>[31]</sup>. This means that the space around the 6a-site is limited. In fact, ionic radius of lanthanum is 1.172 Å with the coordination number equals to 6, which yields the minimum distance of La — O being about 2.57 Å. It is clear that 2.305 Å is insufficient to accommodate La — O. This is why the 6a-site cannot be occupied by lanthanum atoms.

### 3.4 transport property

Sample preparation affects the reliability and accuracy of conductivity measurement. Dense microstructure constituted by grains is a necessary condition for materials to have excellent ionic conductivity. In order to determine the optimal temperature of sintering, dilatometry measurement was performed. The ceramic pellet of  $\text{Ca}_{2.06}\text{La}_{2.61}\square_{0.33}\text{W}_2\text{O}_{12}$  starts to sinter at 1300°C and the optimal temperature of sintering is 1400°C.

The performance and the quality of sintering can be visually displayed by scanning electronic microscopy (SEM), the micrograph of the topographic contrasts for sintered  $\text{Ca}_{2.06}\text{La}_{2.61}\square_{0.33}\text{W}_2\text{O}_{12}$  pellet is shown in **Figure 5**. The compactness of the material was limited by the relatively high porosity, the relative density (measured and calculated from mass-to-

volume ratios) being about 85%. The size of the grains is in the range between 5 — 50  $\mu\text{m}$ . This important grain growth may hinder the sintering process.

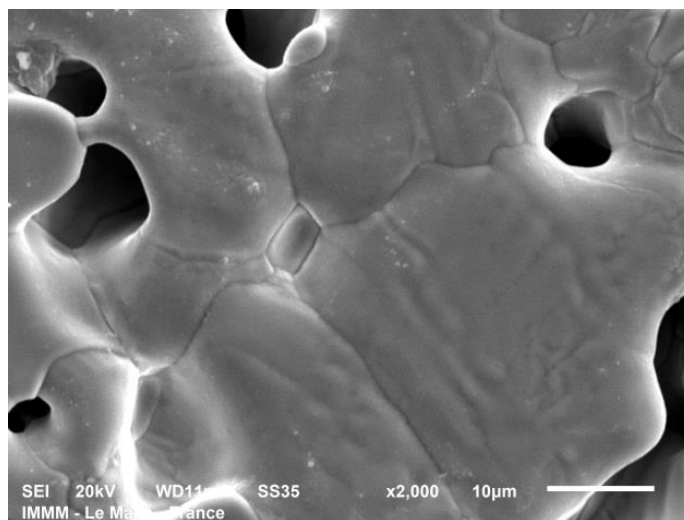


**Figure 5:** Electron micrograph of the polished surface of sintered  $\text{Ca}_2\text{La}_3\text{W}_2\text{O}_{12}$  ceramic pellet.

The conductivity was measured in both dry and wet air atmosphere. The Nyquist plots did not show any polarization at blocking electrodes at low frequency. Nevertheless, the diagrams were analyzed on ZView<sup>[36]</sup>[35] by using equivalent electrical RC circuit, which models electrical behavior of grains and grain boundaries. The two contributions could not be always distinguishable, so we deduced the total conductivities equal to  $1.97 \times 10^{-7} \text{ S cm}^{-1}$  and  $1.39 \times 10^{-7} \text{ S cm}^{-1}$  at  $725^\circ\text{C}$  in dry and wet air atmosphere, respectively. This means the conductivities are not so high and the characteristic frequencies of displacement are low. The Arrhenius plots of the total conductivity considered as the sum of the grain interior and the grain boundary contributions in both dry and wet air atmosphere, are showed in **Figure 6**. The evolutions are almost linear, the related activation energies being  $E_a = 0.67 \text{ eV}$  (dry) and  $E_a = 0.60 \text{ eV}$  (wet).

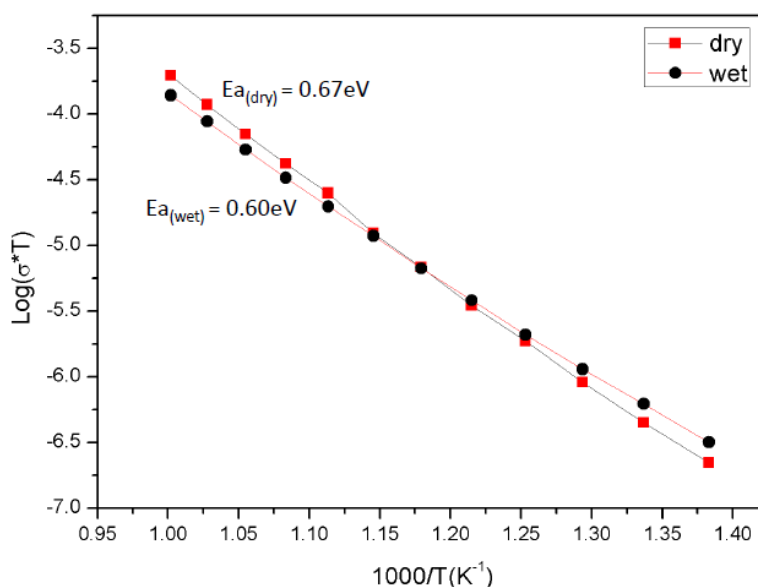


**Figure 6:** Arrhenius plots of the total conductivity in dry (red) and wet (black) air atmosphere.

In summary, the relative density of the ceramic pellet is not sufficiently high (generally > 92% for a good sintering). Additionally, the above calculation of cationic vacancy rate of 4.72% is not satisfactory compared with the 10% anionic vacancy rate of  $\text{La}_2\text{Mo}_2\text{O}_9$  [41]. The illustration of the crystallographic structure of **Figure 4(c)** clearly shows that these vacancies do not form a continuous 3D network because they are arranged in a straight line in the lattices, separated by large distances. **Figure 4(b)** shows that the spaces between the vacancies are filled with many atoms such as Ca, La and W which tend to block the conduction path. The octahedra  $[\text{WO}_6]$  are mutually independent, with neither shared vertex nor shared edge and side. All these factors limit the conductivity of the material. But it is worth noticing that the energy barriers are of 0.67 eV and 0.60 eV for dry and wet air atmosphere, respectively, which are close to the value of 0.68 eV of  $\beta$ - $\text{La}_2\text{Mo}_2\text{O}_9$  at high temperature and smaller than the value of 1.16 eV of  $\alpha$ - $\text{La}_2\text{Mo}_2\text{O}_9$  at low temperature [37].

#### 4. Conclusion

Doping with lower valence cation is an efficient method for finding new compounds having deficient crystallographic structure. In this work, a new cation-deficient Ca-doping lanthanum tungstate was discovered with the exact formula  $\text{Ca}_{2.06}\text{La}_{2.61}\text{W}_{0.33}\text{W}_2\text{O}_{12}$ . The sample was prepared by the conventional solid-state ceramic route. The long thermal treatment at high temperature shows that the kinetic and thermodynamic processes in this compound are very slow. The structure of  $\text{Ca}_2\text{La}_3\text{W}_2\text{O}_{12}$  has been elucidated from microscopy electron diffraction, X-ray and neutron powder diffraction data. The white powder compound crystallizes in the space group  $R\bar{3}C$  (No.167), with  $Z = 18$  and the hexagonal parameters  $a = 9.7747(1)$  Å and  $c = 55.7833(4)$  Å, belonging to a small rare crystallographic family. The transport property was investigated. Due to the insufficient relative density of the pellet and the lack of vacancy leading to the absence of 3D pathways,  $\text{Ca}_{2.06}\text{La}_{2.61}\text{W}_{0.33}\text{W}_2\text{O}_{12}$  presents a weak ionic conductivity in both dry and wet air atmosphere.

#### References

- [1] P. Lacorre, F. Goutenoire, O. Bohnke, R. Retoux and Y. Laligant, Designing fast oxide-ion conductors based on  $\text{La}_2\text{Mo}_2\text{O}_9$ , *Nature*, **404**(2000)856-858.
- [2] F. Goutenoire, O. Isnard, R. Retoux and P. Lacorre, Crystal structure of  $\text{La}_2\text{Mo}_2\text{O}_9$ , a new fast oxide-ion conductor, *Chem. Mater.*, **12**(2000)2575.
- [3] F. Goutenoire, O. Isnard, R. Retoux, O. Bohnke, Y. Laligant and P. Lacorre, Structural and transport characteristics of the LAMOX family of fast oxide-ion conductors, based on lanthanum molybdenum oxide  $\text{La}_2\text{Mo}_2\text{O}_9$ , *J. Mater. Chem.*, **11**(2001)119.
- [4] F. J. Rohr, High-temperature fuel cells in Solid Electrolytes, general principles, characterization, materials, applications, edited by P. Hagenmuller and W. Vangool, (Academic press, New York,1978) p.431.
- [5] J. F. Baumard and P. Abelard, Defect structure and transport properties of  $\text{ZrO}_2$ -based solid electrolytes in Science and technology of zirconia II, edited by A. H. Hever, N. Claussen, M. Ruble, American ceramic society, Columbus, OH(USA), (1983) p.555.
- [6] V. V. Kharton, F. M. B. Marques and A. Atkinson, Transport properties oxide electrolyte ceramics : a brief review, *Solid state ionics*, **174**(2004)135-149.
- [7] S. C. Singhal, Solid oxide fuel cells for power generation, Wiley interdisciplinary review: Energy environ, **3**(2014)179-194.
- [8] E. Wachsman, T. Ishihara and J. Kilner, Low-temperature solid-oxide fuel cells, *MRS Bulletin*, **39**(2014)773-779.
- [9] Z. Shao and W. Zhou, Progress in materials science advanced synthesis of materials for intermediate-temperature solid oxide fuel cells, Elsevier Ltd., **57**(2012)804-874.
- [10] M. J. Reddy, J. E. Svensson, J. Froitzheim, Evaluation candidate materials for balance of plant components in SOFC: oxidation and evaporation properties, *Corrosion Sci.*, **190**(2021)109671.
- [11] I.R. Evans, J.A.K. Howard, J.S.O. Evans, The crystal structure of  $\alpha$ - $\text{La}_2\text{Mo}_2\text{O}_9$  and the structural origin of the oxide ion migration pathway, *Chem. Mater.*, **17**(2005)4074.

- [12] D. Marrero-Lopez, J. pena-Martinez, J. C. Ruiz-Morales and P. Nunez, Phase stability and ionic conductivity in substituted  $\text{La}_2\text{W}_2\text{O}_9$ , *J. of Solid State Chem.*, **181**(2008)253-262.
- [13] Q. F. Fang, X. P. Wang, Z. S. Li, G. G. Zhang and Z. G. Yi, Relaxation peaks associated with the oxygen-ion diffusion in  $\text{La}_{2-x}\text{Bi}_x\text{Mo}_2\text{O}_9$  oxide-ion conductors, *Mater. Sci. eng. A*, **370**(2004)365-369.
- [14] D. Marrero-Lopez, J. Canales-Vazquez, J.C. Ruiz-Morales, J. T. S. Irvine, P. Nunez, Electrical conductivity and redox stability of  $\text{La}_2\text{Mo}_{2-x}\text{W}_x\text{O}_9$  materials, *Electrochimica Acta.*, **50**(2005)4385–4395.
- [15] D. Marrero-Lopez, D. Perez-Coll, J. C. Ruiz-Morales, M. C. Martin-Sedeno and P. nunez, Sythesis and transport properties in  $\text{La}_{2-x}\text{A}_x\text{Mo}_2\text{W}_x\text{O}_{9-6}$  ( $\text{A} = \text{Ca}^{2+}, \text{Sr}^{2+}, \text{Ba}^{2+}, \text{K}^+$ ) series, *Electrochimica Acta.*, **52**(2007)5219-5231.
- [16] G. Corbel, Y. Lalignant, F. Goutenoire, E. Suard and P. Lacorre, Effects of partial substitution of  $\text{Mo}^{6+}$  by  $\text{Cr}^{6+}$  and  $\text{W}^{6+}$  on the crystal structure of the fast oxide-ion conductor structural effects of  $\text{W}^{6+}$ , *Chem. Mater.*, **17**(2005)4678-4684.
- [17] T. D. Vu, F. Krichen, M. Barre, K. Adil, A. Jouanneaux, E. Suard and F. Foutenoire, Crystal structure and ion conduction properties of  $\text{La}_3\text{NbMo}_2\text{O}_{16}$ , *J. of Solid State Chem.*, **237**(2016)411-416.
- [18] M. Yoshimura, A. Rouanet, High temperature phase relation in the system  $\text{La}_2\text{O}_3\text{-WO}_3$ , *Mater. Res. Bull.*, **11**(1976)151.
- [19] Y. Lalignant, A. Le Bail, F. Goutenoire, *Ab Initio* structure determination of Lanthanum Cyclo-tetrate  $\alpha\text{-La}_2\text{W}_2\text{O}_9$  from X-ray and neutron powder diffraction, *J. of Solid State Chem.*, **159**(2001)223-227.
- [20] R. Haugrud, C. Kjølleth, Effects of protons and acceptor substitution on the electrical conductivity of  $\text{La}_6\text{WO}_{12}$ , *J. phys. Chem. solids*, **69**(2008)1758-1765.
- [21] A. Magraso, C. Frontera, D. Marrero-Lopez, P. Nunez, New crystal structure and characterization of lanthanum tungstate " $\text{La}_6\text{WO}_{12}$ " prepared by freeze-drying synthesis, *The royal society of chem.*, (2009)10273-10283.
- [22] M. H. chambrier, A. Le Bail, F. Giovannelli, A. Redjaimia, P. Florian, D. Massiot, E. Suard, F. Goutenoire,  $\text{La}_{10}\text{W}_2\text{O}_{21}$  : An anion-deficient fluorite-related superstructure with oxide ion conduction, *Inorganic chem.*, **53**(2014)147-159.
- [23] T. D. Vu, M. Barre, K. Adil, A. Jouanneaux, E. Suard and F. Goutenoire, Investigation of the  $\text{La}_2\text{O}_3\text{-Nb}_2\text{O}_5\text{-WO}_3$  ternary phase diagram : isolation and crystal structure determination of the original  $\text{a}_3\text{NbWO}_{10}$  material, *J. of Solid State Chem.*, **00**(2015)1-11.
- [24] Solartron materials research and test software, (2004).
- [25] D. Louer and A. Boulitif, Indexing with the successive dichotomy method, *DICVOL04, Z. Krist. Suppl.* **23**(2006)225 - 230.
- [26] T. Degen, M. Sadki, E. Bron, U. König and G. Nenert, The HighScore suite. *Powder Diffr.*, **29**(2014)13-18.
- [27] P. M. de Wolf, A simplified criterion for the reliability of a powder pattern indexing, *Journal of Applied Crystallography*, **1**(1968)108–113.
- [28] M. Klinger and A. Jäger. Crystallographic Tool Box (CrysTBox): automated tools for transmission electron microscopists and crystallographers. *Journal of Applied Crystallography*, **48**(2015).
- [29] A. Le Bail, H. Duroy and J.F. Fourquet, *Ab Initio* structure determination of  $\text{LiSbWO}_6$  by X-ray powder, diffraction, *Mat. Res. Bull.*, **23**(1988)447-452.
- [30] J. Rodriguez-Carvajal, FullProfSuite Program.
- [31] H. A. Mons, M.S. Schriewer, W. Jeitschko, The crystal structure of the isotypic perrhenates  $\text{Ca}_5\text{Re}_2\text{O}_{12}$  and  $\text{Ca}_5\text{Re}_2\text{O}_{12}$ , *J. of solid state chem.*, **99**(1992)149-157.
- [32] T. Hummel, F. Salk, M. Ströbele, D. Enseling, T. Jüstel, H. Meyer, The Orthoperiodates of Calcium, Strontium, and Barium, *Eur. J. Inorg. Chem.* (2015)977–981.
- [33] V. petricek, M. Dusek, L. Palatinus, *Zeitschrift für Kristallographie – Crystalline Materials*, Crystallographic computing system JANA 2006: general features, **229**(2014)345-352.
- [34] W. Pitschke, N. Mattern and H. Hermann, Incorporation of micro-absorption correction into Rietveld analysis, *Powder Diffraction* **8**(1993)223-228.
- [35] I. D. Brown, R.D. Shannon, Empirical bond-strength-bond-length curves for oxides, *Acta Cryst.*, **A29**(1973)266-282.
- [36] **D. Jacobson, ZView, version 3.5h; Scribner Associates, Inc: Southern Pines, NC, ©Copy-right 1996-2019.**
- [37] D. S. Tsai, M. J. Hieh, J. C. Tseng and H. Y. Lee, Ionic conductivities and phase transitions of lanthanide rare-earth substituted  $\text{La}_2\text{Mo}_2\text{O}_9$ , *J. of the european ceramic society*, **25**(2005)481-487.